# The 2020 Sejong Space Geodetic Observatory Local Tie Survey

National Geographic Information Institute, Republic of Korea


December 2020

## Table of contents

# 1. INTRODUCTION

The ITRF is the result of a combination of the different terrestrial reference frames provided by the four main space geodesy techniques GNSS, VLBI, SLR and DORIS. To perform this combination between independent reference frame, it is necessary to have some co-location sites where the various techniques are observing and whose ties have been surveyed in three dimensions.

In this frame, it has been decided to survey Sejong co-location sites (Republic of Korea). Indeed, on this site where three geodetic techniques were currently observing (VLBI, SLR and GNSS). The tie between instrument reference points (i.e., VLBI, SLR. GNSS) was missing and the ties had to be determined.

This document presents the Sejong local tie survey which took place in October 2020, from the observations on site to the computation, with as many details as necessary to fully understand what the resulting SINEX file means.

**Glossary**

ARP : Antenna Reference Point
DORIS : Doppler Orbitography Radiopositioning Integrated by Satellite
GNSS : Global Navigation Satellite System
IERS: International Earth Rotation Service
ITRF : International Terrestrial Reference Frame
IVP : Invariant Point
NGII : National Geographic Information Institute
SINEX : Solution Independent Exchange
SLR : Satellite Laser Ranging
VLBI : Very Long Baseline Interferometry

## 2. CO-LOCATION SITE DESCRIPTION

The Sejong Space Geodetic Observatory is located near Sejong city, approximately 120 km south of Seoul city, the capital city of Republic of Korea.

Figure 1. Location map of VLBI, SLR and GNSS observatory

The VLBI observatory has one 22-meter radio telescope and the SLR observatory also has optical telescope, which are co-located with a permanent IGS GNSS station (SEJN). This site is organized so that five and three reinforced concrete piers surround the VLBI and SLR optical telescopes, respectively. These piers are between 1.6 m and 5.0 m high and their diameters are 0.61m. They are all equipped with self-centering devices and are mostly used for the determination of local tie vector between the geodetic instruments (i.e., VLBI, SLR, GNSS).

Table 1. List of survey marks with DOMES at the Sejong Space Geodetic Observatory

| LOCAL DESIGNATION | GLOBAL/IERS DESIGNATION |
|---|---|
| SEJONG VLBI | 7368 A 2390S001 |
| SEJONG SLR | 7394 A 2390S002 |
| SEJONG GNSS | SEJN A 2390M001 |

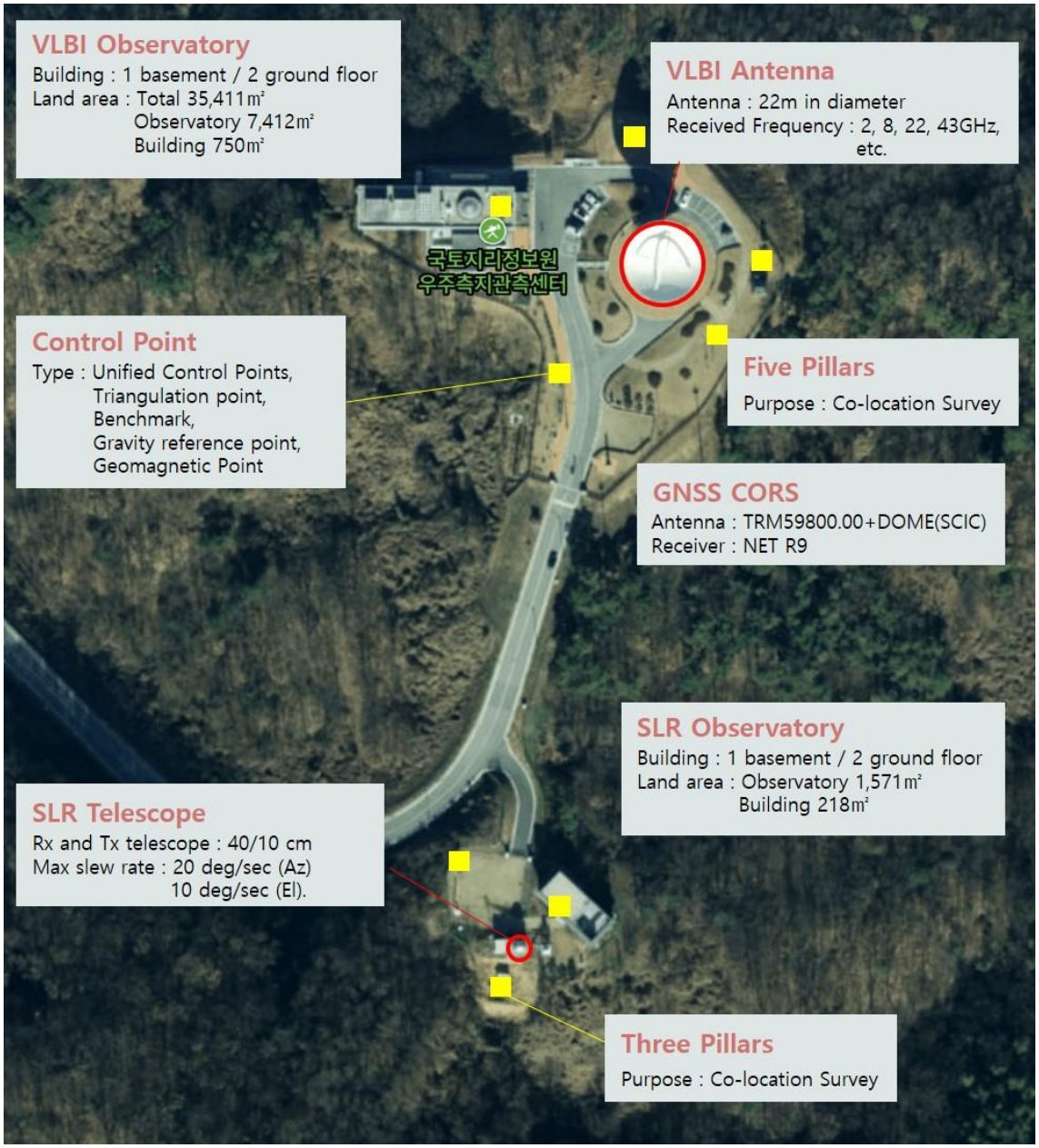


Figure 2. Site description map

A local tie survey was conducted at the observatory in October 2020 by National Geographic Information Institute. Precision classical geodetic observations were combined with geodetic GNSS observations for the purpose of repeat determination of the relationship between the reference points of geodetic instruments (i.e., VLBI IVP 7368 A 2390S001, SLR IVP 7394 A 2390S002, GNSS SEJN A 2390M001, and the surrounding survey controls.

# 3. CO-LOCATED POINTS

## 3.1. VLBI station

The VLBI station was installed at the Sejong Space Geodetic Observatory in March 2012. For the VLBI antenna, the measurement data is received at the phase center of the receiver feed horn. The VLBI reference point (IVP) is the intersection of the azimuth axis with the common perpendicular of the azimuth and elevation axes.

The VLBI IVP was determined by using indirect method. Azimuth and elevation angles of targets on a rigid body were observed from the control points. Then, a least squares adjustment computation was performed to determine the position of VLBI IVP.

| SEJONG | DOMES number 2390S001 7368 |
|---|---|

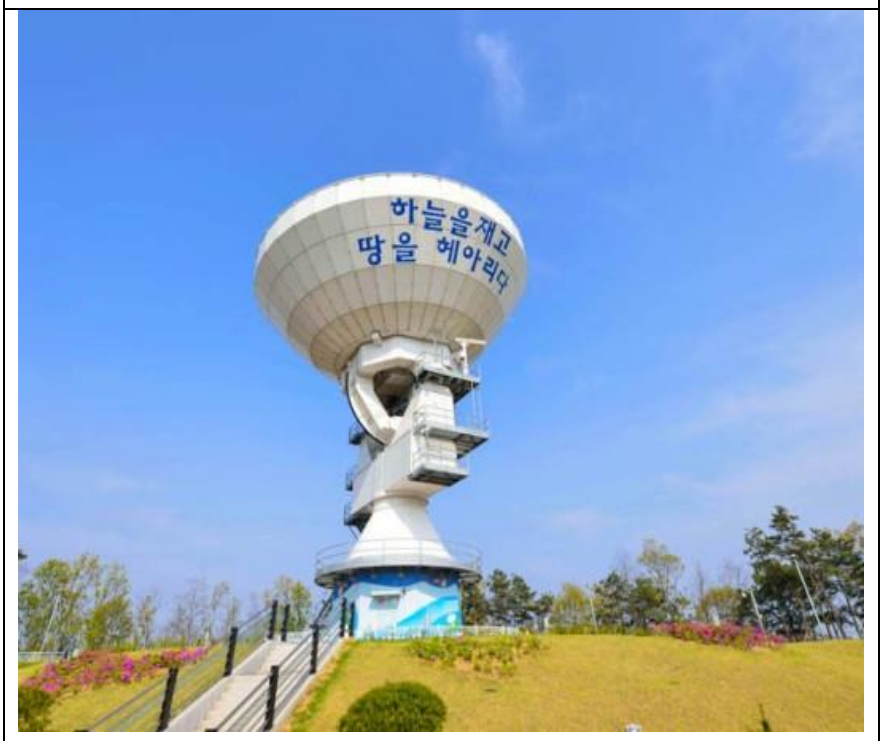


General view

Figure 3. VLBI station installed at Sejong Space Geodetic Observatory

## 3.2. SLR station

The SLR station located approximately 200 m south of VLBI station was installed at the Sejong Space Geodetic Observatory in 2015. Same procedures applied for the estimation of VLBI IVP was adopted to compute the position of SLR IVP.

| SEJONG | DOMES number 2390S001 7394 |
|---|---|

General view

Figure 4. SLR station installed at Sejong Space Geodetic Observatory

## 3.3. GNSS station

A permanent GNSS station named SEJN is continuously operating since February 2012. The antenna is a Trimble TRM 59800.00 type with radome and mounted on top of rigid concrete post.

| Acronym : SEJN | DOMES number : 2390M001 |
|---|---|

General view

Antenna Reference Point

Antenna height is **0.000 m**

Figure 5. GNSS station and ARP

## 3.4. Piers

A network of reinforced concrete piers was set-up. Five and three pillars equipped with self-centering devices has been set up around VLBI and SLR antennas, respectively, to determine the tie between the reference points of geodetic instruments.

VP01

VP02

VP03

VP04

VP05

SP01

SP02

SP03

Figure 6. Pillars for observing targets on VLBI and SLR antennas

# 4. SURVEY DESCRIPTION

The local ties survey of Sejong co-location sites has been carried out by NGII, Republic of Korea. The survey took place from September 28th to October 9th.

## 4.1. Instruments

i. Total Station : TRIMBLE S8
- EDM (infrared) distance standard deviation of a single measurement : 1mm ± 2ppm;
- Angular standard deviation of a mean direction measured in both faces : 1" ± (0.3mgon).

ii. Levelling : TRIMBLE Dini Digital Level
- Accuracy : 0.3mm/km

iii. GNSS : TRIMBLE R8 GNSS, TRIMBLE R10
- Accuracy : 5mm ± 1ppm;
- Dual frequency receivers

## 4.2. Polygon network

All the survey took place to provide the highest accuracy in the determination of the 3D vectors between the observing instruments.

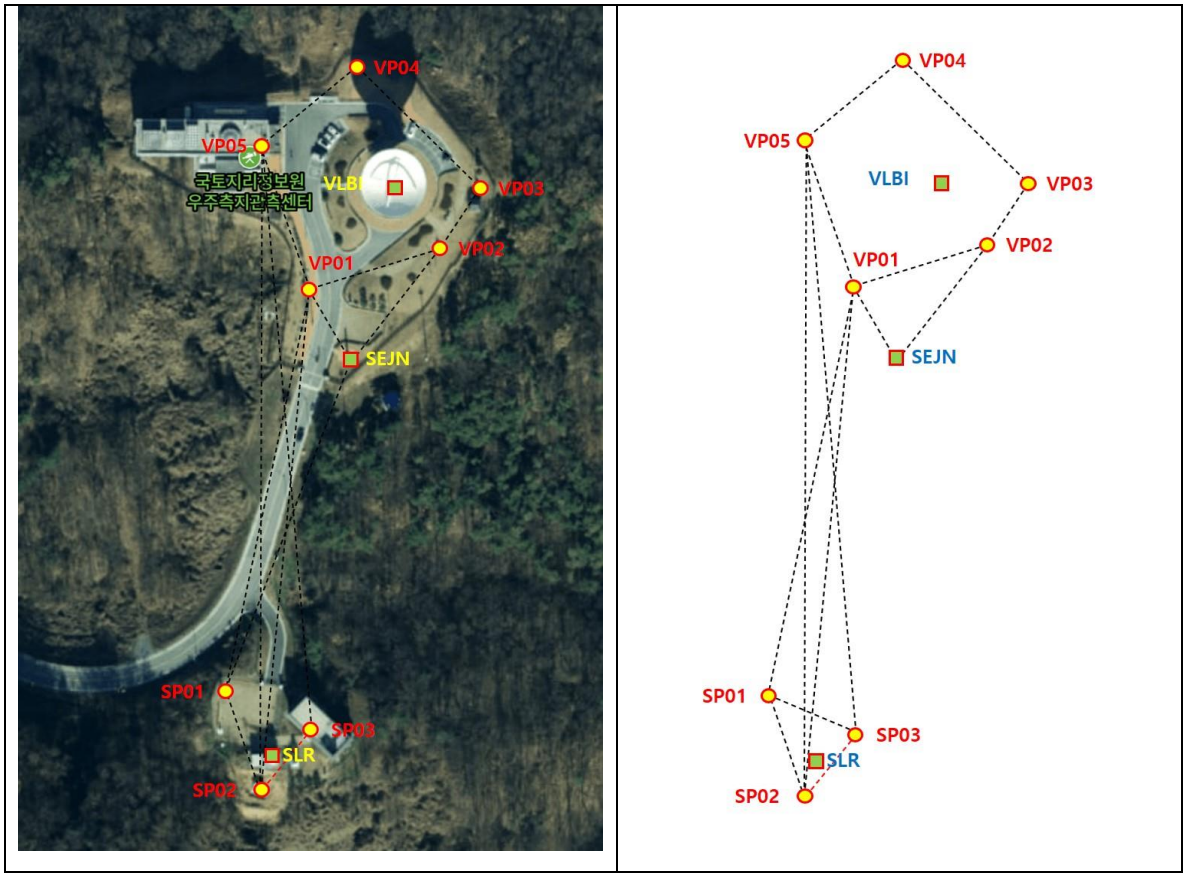


Figure 7. Location map of pillars corresponding polygon network

## 4.3. Survey method

Total station was installed on the top of each pillar, and then horizontal directions and zenith angles of targets were measured. Each set of observed data consists of one reading in both direct and reverse positions. Distances between the points were also measured in both direct and reverse positions. Meteorological data (atmospheric pressure and temperature) were collected during the survey to correct the distances. Forward and backward measurements between the points were obtained by spirit levelling to determine the height differences.

Also, GNSS measurements were collected from the top of each pillars so that transformation parameters could be obtained. The following table sums up the GPS observations with equipment.

Table 2. Description of GNSS datasets collected on pillars

| **Points** | **Period [yy:mn:dd:hh:mm:ss]** | **Receiver** | **Antenna** |
|---|---|---|---|

| | | | |
|---|---|---|---|
| VP01 | 2020:07:31:10:35:00<br>~2020:08:07:09:27:00 | TRIMBLE R10 | TRMR10 |
| VP02 | 2020:07:31:10:36:00<br>~2020:08:07:09:25:00 | TRIMBLE R10 | TRMR10 |
| VP03 | 2020:07:31:10:34:00<br>~2020:08:07:09:24:00 | TRIMBLE R10 | TRMR10 |
| VP04 | 2020:07:31:10:31:00<br>~2020:08:07:09:26:00 | TRIMBLE R10 | TRMR10 |
| VP05 | 2020:07:31:10:42:00<br>~2020:08:07:10:43:00 | TRIMBLE R10 | TRMR10 |
| SP01 | 2020:07:31:10:50:00<br>~2020:08:07:11:07:00 | TRIMBLE R10 | TRMR10 |
| SP02 | 2020:07:31:10:34:00<br>~2020:08:07:09:24:00 | TRIMBLE R10 | TRMR10 |
| SP03 | 2020:07:31:10:53:00<br>~2020:08:03:23:53:00 | TRIMBLE R10 | TRMR10 |

4.3.1. Local ground survey of the pillars and CORS antenna

(a) The origin of the local reference frame will coincide with the CORS SEJN, which is also the origin of the local tie vector. The orientation of the reference frame will be defined by the local geodetic coordinate system of the CORS SEJN.

(b) All possible slant distances and horizontal and vertical angles be- tween the pillars are to be observed with a total station (an electronic theodolite integrated with an electronic distance measuring instrument).

(c) Only horizontal and vertical angles will be measured from the pillars to the antenna reference point (ARP) of the CORS. Slant distance will not be measured to the ARP, since it is not feasible to mount a glass-prism reflector at the ARP.

(d) Moreover, since it is not possible to center a target on the ARP, the horizontal and vertical angles will be measured to the bottom-left and bottom-right of the antenna, and their average will be used as a measurement to the ARP.

4.3.2. GNSS survey of the pillars and CORS antenna

Determine ITRF coordinates of the eight pillars and the CORS ARP from the following data:

- A GNSS survey campaign will be performed by collecting data simultaneously from GNSS receivers mounted on all eight pillars and the CORS SEJN.
- Data will be collected at a 30-sec rate over seven 24-hour sessions (one week).
- The GNSS data collected at the pillars will be processed along with GNSS data from 51 IGS stations around the world, resulting in a set of GNSS vectors aligned to ITRF 2014 (Altamimi et al., 2017). The resulting vectors, and their covariance matrix, will be used as observational data in the subsequent network adjustment described below.

4.3.3. Network adjustment of local survey and GNSS data

(a) A simultaneous 3D network adjustment of the local survey and GNSS data will be performed to determine the coordinates of all pillars. In so doing, the published IGS coordinates of the CORS SEJN will be held fixed to overcome the datum deficiency (of three) and to yield a minimally constrained least-squares solution.

(b) Additionally, an over-constrained adjustment will be performed by imposing stochastic constraints on the coordinates of all IGS stations (except for SEJN, which will be held fixed), the variances of which will be taken from IGS published values. Statistical analysis will be performed to decide upon which of the two adjustments to adopt finally. At this time we conjecture that any difference in scale or orientation between the two adjustments would have an insignificant impact on the tie vector, since it emanates from the same fixed point in both adjustment, and it is relatively short in length (compared to the scale of the adjusted network).

(c) The adopted adjustment will result in estimated coordinates for the CORS SEJN and all pillars in the ITRF 2014 coordinate frame. Obviously, these coordinates can also be expressed in the local geodetic coordinate system of the CORS SEJN, which might be convenient for the work described in the following.

4.3.4. Survey of targets mounted on the VLBI antenna

(a) Thirteen targets were mounted on the VLBI antenna.

(b) Using a total station, all possible distances from each of the five pillars to the targets on the antenna will be measured. The targets consist of 7 prisms and 6 sheet targets at different location on VLBI antenna.

(c) The elevation angle of the VLBI antenna remained constant at 90 degrees for all measured horizontal angles.

(d) It is expected that, during rotations through any given vertical plane, only two targets can be seen clearly throughout the entire movement of the antenna, as the other targets will be obscured by the antenna body itself.

(e) All possible horizontal and vertical angles between the pillars and the VLBI targets will be measured.

(f) The coordinates of the targets, along with their covariance matrix, were estimated via a least-squares adjustment of the data. A minimally constrained adjustments were performed first, using partial MINOLESS to minimize the changes in coordinates of the pillars. A second adjustment was performed by imposing stochastic constraints on the coordinates of the pillars.

4.3.5. Local ground survey of SLR telescope

(a) Similar surveying procedures were conducted on the SLR telescope from two pillars.

(b) Three concrete pillars were installed around the SLR telescope. But measurements could only be taken from two pillars located on opposite sides of the telescope (SP02 and SP03). One of the pillars (SP01) were used as a backsight only, because its height was lower than the telescope, preventing observations to the telescope from being made.

4.3.6. Apply TLS approach to estimate the IVP

(a) The principal parameters to estimate are the coordinates of IVP in the local frame.

(b) The residuals of target coordinates were predicted as a byproduct. Their magnitudes should be both reflective of the quality of the preceding adjustments and the validity of the functional models used to relate the target coordinates to the geometric parameters of the circles and cones.

# 5. Computation

The overall procedures to estimate the IVPs can be represented by Fig. 5.1 and more details are as follows.

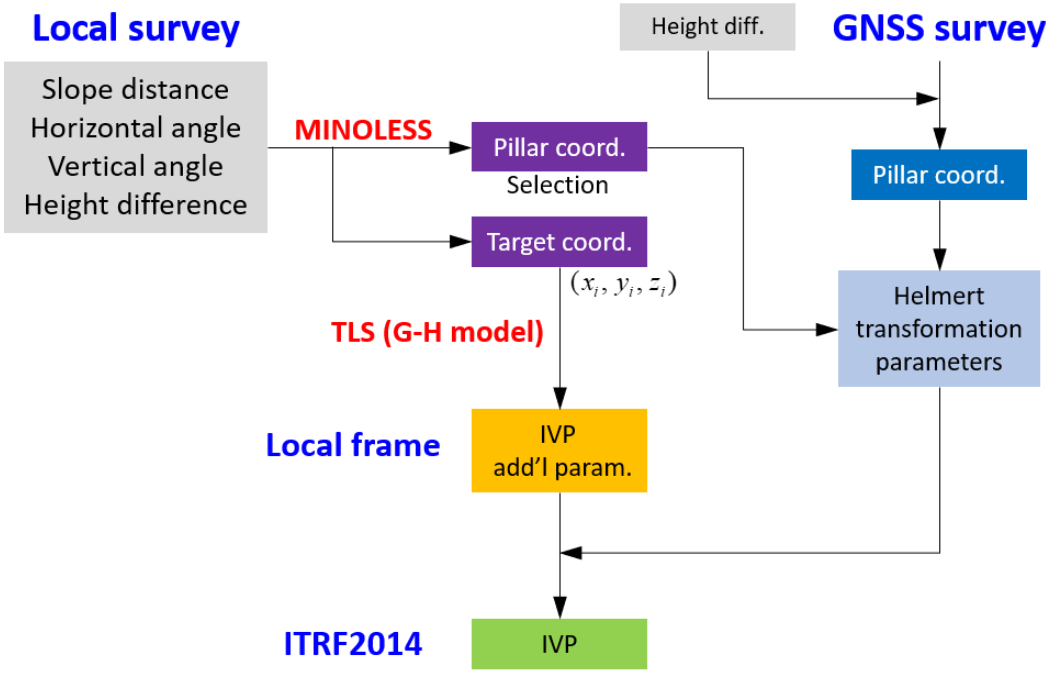


Figure 8. Overall procedures to estimate the IVPs

## 5.1. Local surveying

### 5.1.1. Description of the site

(a) The local survey involves measurements between the five pillars and the GNSS CORS antenna at station SEJN.

(b) The slope distances as well as horizontal and vertical angles measured with a total station are considered.

(c) The GNSS CORS (SEJN) was set to be at the origin of the local coordinate system, which was eventually the origin for the local tie vector to the IVP

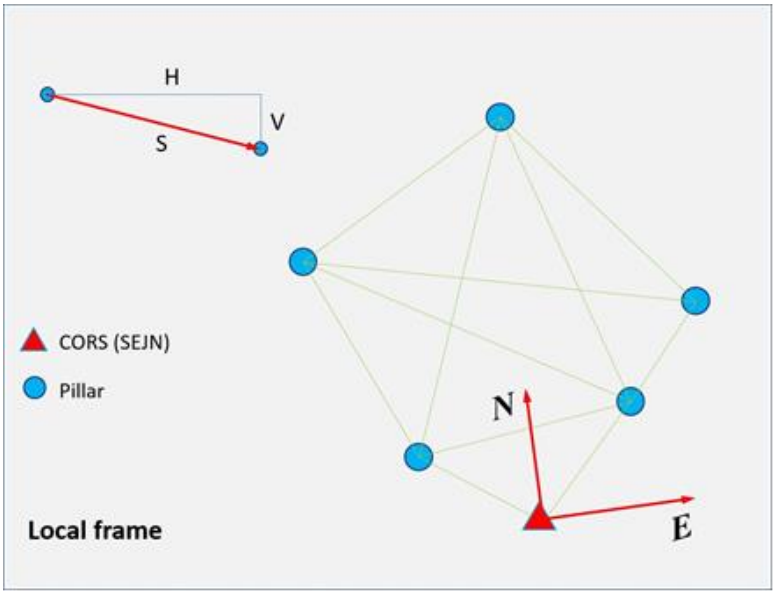


Figure 9. Local coordinate frame of the site

5.1.2. Determination of local frame

(a) The local reference frame can be determined by local survey between Pillars and CORS SEJN.

(b) Local survey includes slope distance, horizontal and vertical angles, height difference from leveling network.

(c) Measure all possible combinations of measurements between the pillars and the CORS antenna.

(d) Perform a 3D network adjustment of these data using MINOLESS technique to determine local frame, which does not require any constraints.

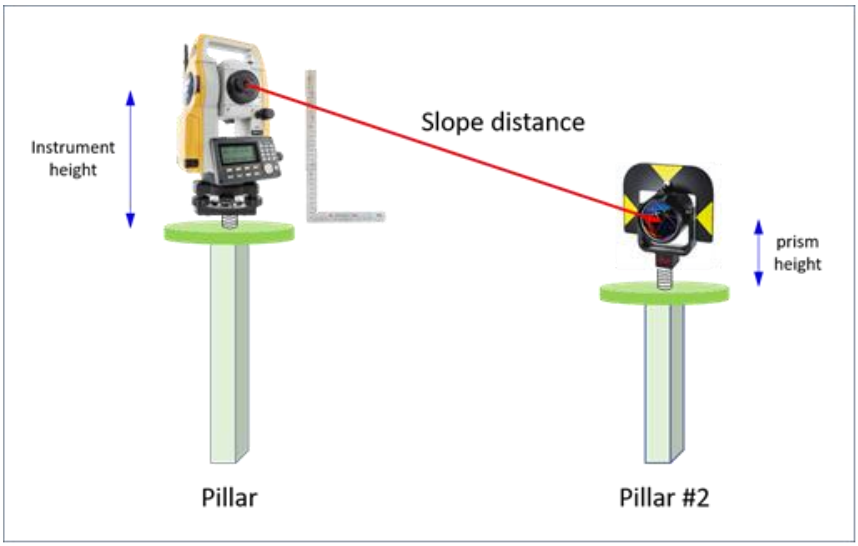


Figure 10. Schematic diagram of local surveying with a total station

5.1.3. Local coordinates of the targets

(a) Similar local surveying was conducted for the targets on VLBI antenna.

(b) Slope distance and vertical angle is measured to each target.

(c) Horizontal angles were observed between the pillars and the targets.

(d) The coordinates of the targets were estimated based on the coordinates of the pillars in the local frame, which were used as observations to determine IVP using TLS approach.

## 5.2. Estimation of IVPs of VLBI and SLR antennas

5.2.1. Motion of VLBI antenna

(a) All targets are located on the “outside” of the VLBI antenna opposite side of the concave area).

(b) Two different motions are possible for the VLBI antenna.

- Azimuthal rotation through 360 degrees

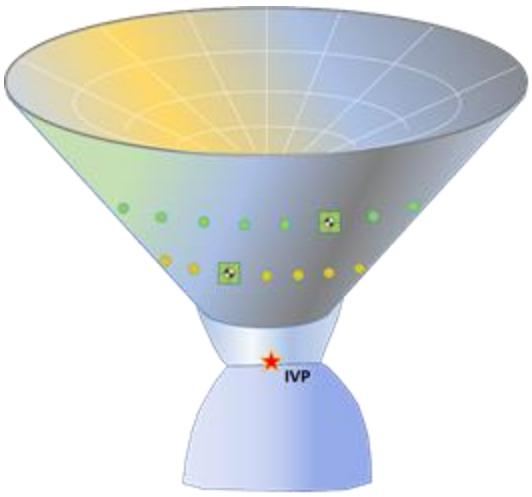


Figure 11. Azimuth rotation – showing two targets are their traces during rotation

- Rotation in elevation (i.e., in a vertical plane) by 90 degrees, from zenith to the horizon, at any azimuth.

(c) By combining the azimuthal rotation and the rotations in elevation, we can measure many locations in 3D for each target.

(d) However, the targets on the surface of the antenna are generally not visible for zenith angles greater than 40 degrees, thus the actual number of measurements will be less.

5.2.2. The azimuthal rotation for IVP estimation

(a) Assume the local frame and the VLBI frame have been aligned to each other.

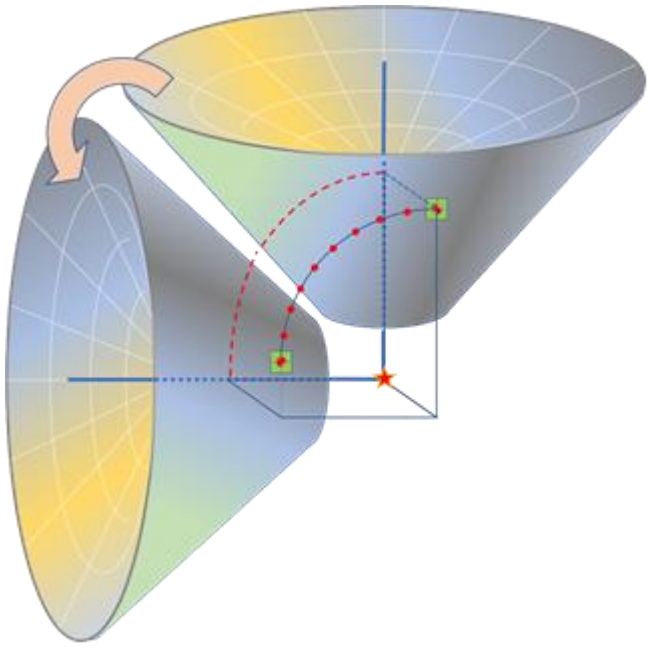

Figure 12. Rotation in elevation (i.e., in a vertical plane)

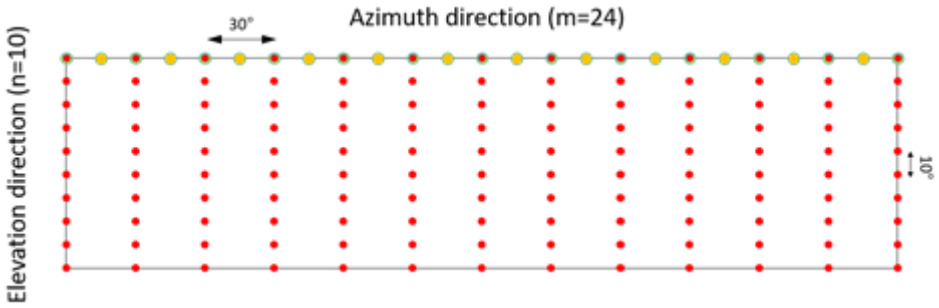


Figure 13. 3D location for each target, depicted as a grid

(b) The azimuthal rotation of the targets is depicted in Figure 13, where the trace of two targets are shown to generate concentric circles with different heights, the centers of which have horizontal coordinates that coincide with those of the IVP.

(c) The radii of the circles are different from each other depending on the location of the target.

(d) Since the radius of the horizontal circle ($r_k$) and the height of the plane ($\gamma_k$) are highly correlated to each other, it is desirable to estimate the radius of the circle only using the horizontal components.

(e) Therefore, the mathematical model for the circle traced by target $k$, through points $(x_i, y_i, z_i)$, at height $r_k$ can be expressed by

$$R_k(\alpha, \beta, \gamma_k) = (x_i - \alpha)^2 + (y_i - \beta)^2 - r_k^2 = 0$$

Where $r_k$ is the radius of the traced circle centered at $(\alpha, \beta)$.

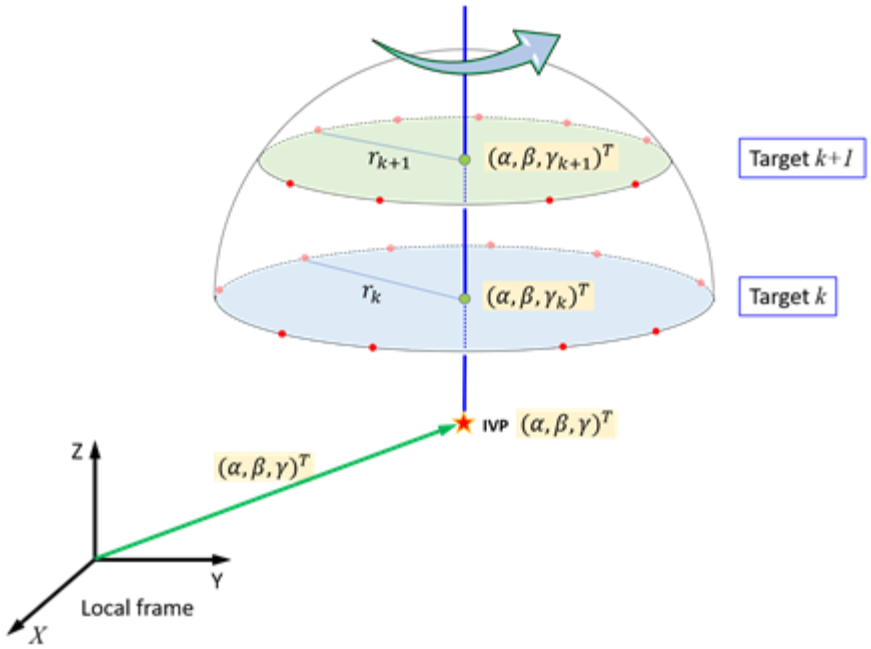


Figure 14. The azimuthal trace of two targets

5.2.3. The rotation of targets in elevation

(a) The targets are generally offset from the vertical plane of rotation through the IVP.

(b) Since the rotations through a vertical plane cause the axis of the antenna to move from zenith to horizon, the targets will trace a quarter circle with its center on the rotation axis.

(c) The radii of the traced circles will be different for each target depending on the orthogonal distance between the vertical plane it traces and the parallel vertical plane that contains the IVP.

(d) The center of each quarter circle will be located on the same horizontal plane that passes through the IVP.

(e) The mathematical model for the circle traced by vertical rotation can be represented by

$$C_\ell(\alpha_\ell, \beta_\ell, \gamma, b_\ell) = (x_i - \alpha_\ell)^2 + (y_i - \beta_\ell)^2 + (z_i - \gamma)^2 - b_\ell^2 = 0$$

Where $b_\ell$ is the radius of the quarter circle centered at $(\alpha_\ell, \beta_\ell, \gamma)$ and traced by target $\ell$, through points $(x_i, y_i, z_i)$, while rotating in a vertical plane.

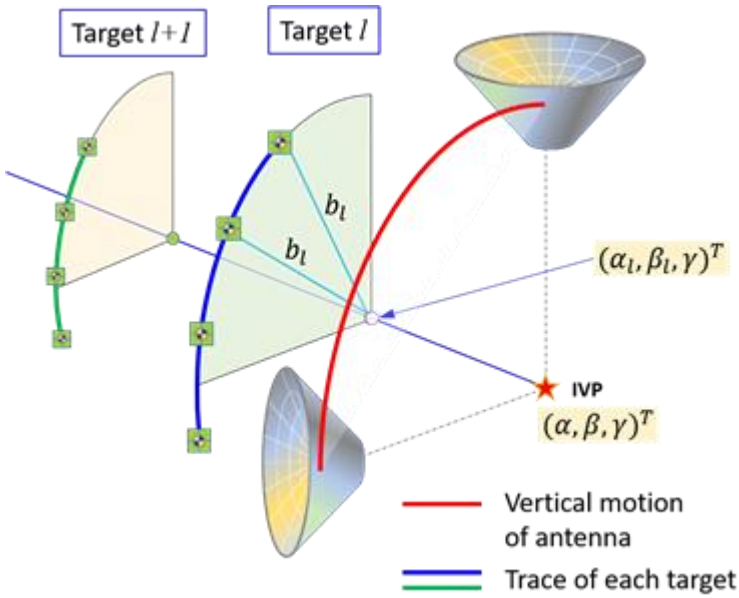


Figure 15. The rotation of targets in elevation (perspective view)

- However, the radius of the vertical quarter-circle $(b_\ell)$ is correlated to the height components of IVP $(\gamma)$, which makes the system unstable to estimate.
- Instead of estimating the radius and the horizontal components of the quarter-circle, we had better estimate the slant height of a cone with the apex at IVP (see Figure 16).
- Therefore, the mathematical model for the vertical rotation of target $\ell$ should be slightly modified to form of a distance between the IVP and the observed targets.

$$C_\ell(\alpha, \beta, \gamma, c_\ell) = (x_i - \alpha_\ell)^2 + (y_i - \beta_\ell)^2 + (z_i - \gamma)^2 - c_\ell^2 = 0$$

Where $c_\ell$ is the slant height of the cone made up by the vertical rotation about the apex at the IVP.

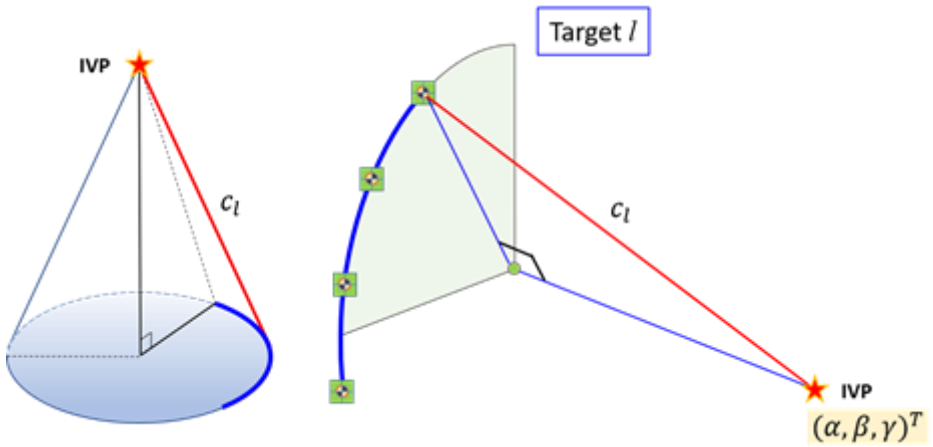


Figure 16. The rotation of targets in elevation represented by a cone with the apex at IVP

- Since the horizontal coordinates of the IVP $(\alpha,\beta)$ are well controlled by observations made using the horizontal rotation, it is expected that the vertical coordinates $(\gamma)$ of the IVP and the slant height of the cone $(c_\ell)$ can also be determined well, too.

5.2.4. Applying Total Least Squares

By Total Least Squares (TLS), we refer to a least-squares estimator that minimizes the random errors in all the data variables (Schaffrin and Snow, 2010). This is in contrast to a least-squares estimator within a model that considers only the dependent variables of the model to be contaminated by random errors, treating the independent variables as error free.

(a) The coordinates of the targets mounted on the VLBI antenna can be estimated from surveying data such as slope distances, horizontal and vertical angles.

(b) Then, we can apply the TLS method to estimate the IVP coordinates based on the coordinates of the targets.

(c) In summary, the mathematical model is composed of two equations: one that pertains to a full circle in a horizontal plane due to azimuthal rotation and another that pertains to a slant height of a cone due to rotations within vertical planes. Thus, two equations of primary interest are as follows:

$$R_k(\alpha,\beta,r_k)=(x_i-\alpha)^2+(y_i-\beta)^2-r_k^2=0$$

$$C_\ell(\alpha,\beta,\gamma,c_\ell)=(x_i-\alpha)^2+(y_i-\beta)^2+(z_i-\gamma)^2-c_\ell^2=0$$

(d) The unknown parameters of the model are summarized as follows:

- The three IVP coordinates, being the only parameters of interest: $\alpha$, $\beta$, and $\gamma$.

- $n_k$ number of nuisance parameters related to the azimuthal rotation, that is, radii of the horizontal circles: $r_k\,(k=1,...,n_k)$, where $n_k$ is the number of targets.
- $n_\ell$ number of nuisance parameters related to quarter circles due to rotations through vertical planes, that is, the slant heights of the cones: $c_\ell\,(\ell=1,...,n_\ell)$ where $n_\ell$ is the number of targets related to vertical rotation.

## 5.3. Helmert transformation to ITRF2014

(a) Since the IVP should be represented in ITRF2014, the transformation parameters should be estimated.

(b) Considering the numerical stability, it would be better to estimate the transformation parameters in North-East-Up (NEU) frame referring to GNSS CORS as its origin.

(c) A well-known relationship between reference frames can be found in IERS webpage, while the velocity components are neglected in this experiment (Jekeli, 2016).

$$\begin{bmatrix} x_2 \\ y_2 \\ z_2 \end{bmatrix} = \begin{bmatrix} x_1 \\ y_1 \\ z_1 \end{bmatrix} + \begin{bmatrix} T_x \\ T_y \\ T_z \end{bmatrix} + s \begin{bmatrix} x_1 \\ y_1 \\ z_1 \end{bmatrix} + \begin{bmatrix} 0 & R_z & -R_y \\ -R_z & 0 & R_x \\ R_y & -R_x & 0 \end{bmatrix} \begin{bmatrix} x_1 \\ y_1 \\ z_1 \end{bmatrix}$$

(e) The transformation parameters are estimated by conventional Least-Squares adjustment and the estimated parameters are applied for the transformation of IVPs coordinates and their variance-covariance matrix.

# 6. RESULTS

## 6.1. Estimated coordinates of pillars and targets

(a) The Partial MINOLESS (PMINOLESS) based on traverse surveying between VLBI/SLR pillars and GNSS CORS (SEJN) is given in Table 3 and table 4 (Snow, 2002). In this case, the norm of updates for 9 pillars (5 VLBI, 3 SLR, and GNSS) are minimized.

Table 3. The partial MINOLESS of traverse surveying

| Item | Value |
|---|---|
| Slant distance | 42 |
| Horizontal angle | 28 |
| Vertical angle | 46 |
| Height difference | 8 |
| Total unknown parameters $(m)$ | 27 |
| Observations $(n)$ | 124 |
| Model redundancy $(n-rkA)$ | 101 |
| Datum deficiency $(m-rkA)$ | 4 |

Table 4. The estimated coordinates and standard deviations of PMINOLESS for traverse surveying

| PID | $x\,[mm]$ | $y\,[mm]$ | $z\,[mm]$ | $\sigma_x[mm]$ | $\sigma_y[mm]$ | $\sigma_z[mm]$ |
|---|---|---|---|---|---|---|
| SEJN | 7.1593 | -26.3106 | 181.1949 | 5.5 | 10.0 | 0.1 |
| VP01 | -0.0018 | 0.0019 | 177.9076 | 0.9 | 1.6 | 0.2 |
| VP02 | 46.5291 | -0.0006 | 180.8368 | 0.9 | 2.4 | 0.2 |
| VP03 | 64.9451 | 15.4677 | 180.9529 | 1.3 | 2.2 | 0.1 |
| VP04 | 38.0171 | 65.5437 | 180.5820 | 0.5 | 2.1 | 0.1 |
| VP05 | 1.0574 | 50.7581 | 185.5902 | 1.3 | 1.6 | 0.1 |
| SP01 | -65.1482 | -121.5971 | 173.9719 | 0.8 | 0.8 | 0.2 |
| SP02 | -62.8033 | -156.9987 | 179.3986 | 1.2 | 0.9 | 0.2 |
| SP03 | -41.1280 | -142.0817 | 181.3185 | 1.0 | 1.1 | 0.2 |

(b) The Partial MINOLESS (PMINOLESS) of pillars along with all targets on antenna/telescope is estimated by selecting 9 pillars (5 VLBI, 3 SLR, GNSS). See Tables 5 and 6.

Table 5. The partial MINOLESS of all targets

| Item | Value |
|---|---|
| Slant distance | 4080 |
| Horizontal angle | 3406 |
| Vertical angle | 4085 |
| Height difference | 8 |
| Total unknown parameters $(m)$ | 6618 |
| Observations $(n)$ | 11579 |
| Model redundancy $(n-rkA)$ | 4965 |
| Datum deficiency $(m-rkA)$ | 4 |

Table 6. The estimated coordinates and standard deviations of PMINOLESS for all targets including pillars

| PID | $x\,[mm]$ | $y\,[mm]$ | $z\,[mm]$ | $\sigma_x[mm]$ | $\sigma_y[mm]$ | $\sigma_z[mm]$ |
|---|---|---|---|---|---|---|
| SEJN | 7.1650 | -26.3146 | 181.1952 | 65.8 | 118.8 | 1.2 |
| VP01 | 0.0007 | -0.0033 | 177.9093 | 6.1 | 4.0 | 0.9 |
| VP02 | 46.5336 | 0.0001 | 180.8354 | 6.1 | 3.8 | 0.9 |
| VP03 | 64.9513 | 15.4750 | 180.9523 | 3.6 | 6.8 | 0.9 |
| VP04 | 38.0160 | 65.5485 | 180.5833 | 4.7 | 2.4 | 0.9 |
| VP05 | 1.0542 | 50.7564 | 185.5904 | 2.3 | 3.8 | 0.9 |
| SP01 | -65.1544 | -121.5988 | 173.9722 | 1.6 | 1.0 | 1.5 |
| SP02 | -62.8039 | -156.9996 | 179.3976 | 5.2 | 1.2 | 1.5 |
| SP03 | -41.1299 | -142.0849 | 181.1952 | 3.2 | 3.9 | 1.5 |
| PH01 000 90 | 42.0311 | 25.9128 | 196.4277 | 3.0 | 3.7 | 2.6 |
| PH01 015 90 | 42.5024 | 24.6831 | 196.4281 | 3.1 | 3.7 | 2.6 |
| PH01 030 90 | 42.6418 | 23.3756 | 196.4284 | 3.3 | 3.7 | 2.6 |
| PH01 045 90 | 42.4387 | 22.0771 | 196.4294 | 3.4 | 3.7 | 2.6 |
| ⋮ | ⋮ | ⋮ | ⋮ | ⋮ | ⋮ | ⋮ |
| SV08 340 05 | -55.5802 | -149.5825 | 176.7803 | 3.8 | 3.8 | 3.7 |
| SV08 340 10 | -55.5787 | -149.6084 | 176.7380 | 3.8 | 3.8 | 3.7 |
| SV08 340 20 | -55.5763 | -149.6485 | 176.6470 | 3.8 | 3.8 | 3.7 |
| SV08 340 30 | -55.5747 | -149.6717 | 176.5505 | 3.8 | 3.8 | 3.7 |

## 6.2. Estimated IVPs with nuisance parameters

The estimated IVPs of VLBI and SLR together with nuisance parameters are shown in Tables 7 and 8, respectively.

Table 7. The estimated parameters along with the initial approximations for the IVP of VLBI antenna

| $\xi$ | $\xi_i^0\ [m]$ | $\hat{\xi}_i\ [m]$ | $\sigma_{\hat{\xi}_i}\ [mm]$ |
|---|---|---|---|
| $\alpha$ | 37.6 | 37.6311 | 0.2 |
| $\beta$ | 23.5 | 23.4885 | 0.2 |
| $\gamma$ | 194.0 | 194.5947 | 0.7 |
| $r_1$ | 5.0 | 5.0152 | 0.7 |
| $r_2$ | 5.0 | 5.0184 | 0.6 |
| $r_3$ | 5.0 | 5.0136 | 0.8 |
| $r_4$ | 5.0 | 5.0134 | 0.7 |
| $r_5$ | 4.0 | 3.8817 | 0.7 |
| $r_6$ | 4.0 | 3.8822 | 0.7 |
| $r_7$ | 4.0 | 3.8865 | 0.7 |
| $r_8$ | 4.5 | 4.7494 | 0.2 |
| $r_9$ | 4.7 | 4.7519 | 0.3 |
| $r_{10}$ | 5.0 | 5.1286 | 0.8 |
| $r_{11}$ | 5.0 | 5.1335 | 0.9 |
| $c_1$ | 4.0 | 5.3395 | 0.4 |
| $c_2$ | 4.0 | 5.3418 | 0.4 |
| $c_3$ | 4.0 | 5.3378 | 0.7 |
| $c_4$ | 4.0 | 5.3380 | 0.6 |
| $c_5$ | 4.0 | 4.2965 | 0.7 |
| $c_6$ | 4.0 | 4.2925 | 0.4 |
| $c_7$ | 4.0 | 4.2955 | 0.4 |
| $c_{12}$ | 4.0 | 3.9918 | 0.6 |
| $c_{13}$ | 4.0 | 3.9984 | 0.7 |

Table 8. The estimated parameters along with the initial approximations for the IVP of SLR telescope

| $\xi$ | $\xi_i^0\ [m]$ | $\hat{\xi}_i\ [m]$ | $\sigma_{\hat{\xi}_i}\ [mm]$ |
|---|---|---|---|
| $\alpha$ | -55.5 | 55.4450 | 0.5 |
| $\beta$ | -149.0 | -149.1033 | 0.4 |
| $\gamma$ | 176.6 | 176.4670 | 1.0 |
| $r_1$ | 0.55 | 5.0152 | 1.1 |
| $r_2$ | 0.55 | 5.0184 | 1.1 |
| $c_3$ | 0.60 | 0.6527 | 0.8 |
| $c_4$ | 0.60 | 0.6565 | 0.8 |
| $c_5$ | 0.68 | 0.8057 | 1.0 |
| $c_6$ | 0.68 | 0.7897 | 1.0 |
| $c_7$ | 0.60 | 0.6125 | 0.7 |
| $c_8$ | 0.60 | 0.5922 | 0.8 |

## 6.3. Helmert 7-parameter transformation

The IVPs of VLBI and SLR in local frame are transformed to ITRF2014 via Helmert 7-parameter transformation. The estimated parameters for the transformations are presented in Table 9.

Table 9. Estimated parameters (Helmert 7-parameter transformation)

| | Parameter | Value | $\sigma$ |
|---|---|---|---|
| Translation [mm] | $T_x$ | -14297.723 | 69.907 |
| | $T_y$ | 23182.330 | 22.034 |
| | $T_z$ | -181182.809 | 12.988 |
| Rotation [arcsec] | $R_x$ | 9.58682 | 24.914 |
| | $R_y$ | 34.60531 | 79.667 |
| | $R_z$ | -0.00001 | 7.905 |
| Scale [ppm] | $s$ | -85.71575 | 34.617 |

## 6.4. IVPs of VLBI and SLR, and ARP of SEJN GNSS station in ITRF2014

The results of IVPs of VLBI and SLR, and ARP of SEJN GNSS station in ITRF2014 are shown in SINEX format (IERS, 2006) as follows:

```
%=SNX 2.10 NGI 20:320:00000 NGI 20:213:00000 20:290:00000 C 00009 2
*-------------------------------------------------------------------------------
+FILE/COMMENT
* File created by Space Geodetic Observation Center (Sejong, Korea)
* Matrix Scalling Factor used: 1.0000000000
* Contact: Dr. Sang-Oh Yi
-FILE/COMMENT
*-------------------------------------------------------------------------------
+SITE/ID
*CODE PT __DOMES__ T _STATION DESCRIPTION__ APPROX_LON_ APPROX_LAT_ _APP_H_
 7368  A 23907S001 C 22m VLBI               127 18 12.1  36 31 21.8   194.6
 7394  A 23907S002 C SLR telescope          127 18 10.5  36 31 15.6   176.5
 SEJN  A 23907M001 C Sejong, Korea          127 18 11.5  36 31 20.0   181.2
-SITE/ID
*-------------------------------------------------------------------------------
+SOLUTION/EPOCHS
*Code PT SOLN T Data_start__ Data_end____ Mean_epoch__
-SOLUTION/EPOCHS
*-------------------------------------------------------------------------------
+SOLUTION/ESTIMATE
*INDEX TYPE__ CODE PT SOLN _REF_EPOCH__ UNIT S __ESTIMATED VALUE____ _STD_DEV___
     1   STAX 7368  A    1 20:290:00000 m    2 -3.110080208076968E+06 3.219499E-04
     2   STAY 7368  A    1 20:290:00000 m    2  4.082066591964328E+06 3.979317E-04
     3   STAZ 7368  A    1 20:290:00000 m    2  3.775076757937167E+06 3.826499E-04
     4   STAX 7394  A    1 20:290:00000 m    2 -3.110108532334689E+06 3.448585E-04
     5   STAY 7394  A    1 20:290:00000 m    2  4.082170267091798E+06 3.742187E-04
     6   STAZ 7394  A    1 20:290:00000 m    2  3.774911767172587E+06 4.261244E-04
     7   STAX SEJN  A    1 20:290:00000 m    2 -3.110082023640000E+06 1.172608E-03
     8   STAY SEJN  A    1 20:290:00000 m    2  4.082093867720000E+06 1.311069E-03
     9   STAZ SEJN  A    1 20:290:00000 m    2  3.775023462800000E+06 1.395240E-03
-SOLUTION/ESTIMATE
*-------------------------------------------------------------------------------
+SOLUTION/MATRIX_ESTIMATE L COVA
*PARA1 PARA2 ____PARA2+0__________ ____PARA2+1__________ ____PARA2+2__________
     1     1  1.036517456325420E-07
     2     1 -1.028585257151120E-07  1.583496046558640E-07
     3     1 -9.024215670926040E-08  1.183496686777440E-07  1.464209791676170E-07
     4     1 -1.713304926907030E-08  2.096128644018040E-08  2.304177033209090E-08
     4     4  1.189273570059940E-07
     5     1  2.232830083403650E-08 -2.685445361421650E-08 -3.115584361357390E-08
     5     4 -8.004857973575680E-08  1.400396084192140E-07
     6     1  2.148086068125000E-08 -3.101923314340830E-08 -2.059343630259590E-08
     6     4 -3.522072125910830E-08  3.922502715440640E-08  1.815820366503760E-07
     7     1 -2.379594810031460E-08  7.751050709719020E-09  2.081683745484740E-09
     7     4 -1.501088522826610E-08 -4.519199800308460E-10 -2.660929211063880E-08
     7     7  1.375009990221280E-06
     8     1  7.448324160324740E-09 -2.902278837506500E-08 -5.751687539098320E-10
     8     4 -1.143300332855890E-08  7.112402745482130E-09  1.342838069288290E-08
     8     7  2.920199672844750E-07  1.718902465425990E-06
     9     1  6.962733625583170E-09 -8.106740682517070E-09 -3.998757160557580E-08
     9     4 -2.560348384338040E-08  2.568007407287700E-08 -4.756699932091870E-09
     9     7  4.715468967099470E-07 -1.160205507221590E-06  1.946693715474460E-06
-SOLUTION/MATRIX_ESTIMATE L COVA
%ENDSNX
```

# 7. REFERENCES

Altamimi, Z., Rebischung, P., Métivier, L. and Collilieux, X. (2017), Analysis and results of ITRF2014, IERS Technical Note No. 38.

IERS (2006), SINEX Version 2.02, IERS Message No. 103, https://www.iers.org/SharedDocs/Publikationen/EN/IERS/Documents/ac/sinex/messaga_103.txt.txt?__blob=publicationFile&v=1.

Jekeli, C. (2016), Geometric Reference Systems in Geodesy, The Ohio State University.

Schaffrin, B and Snow, K. (2010), Total Least-Squares regularization of Tykhonov type and an ancient racetrack in Corinth, Linear Algebra and its Applications, 432, pp. 2061-2076.

Snow, K. (2002). Applications of parameter estimation and hypothesis testing to GPS network adjustments. Master's thesis, The Ohio State University.